Wind-vector estimation for RADARSAT-1 SAR images

Wind Vector Estimation for RADARSAT-1 SAR Images: Validation of wind direction estimates based upon geometry diversity

Qingping Zou, Yijun He, *Member, IEEE*, Will Perrie, and Paris W. Vachon, *Senior Member, IEEE*

***Abstract*—A new wind vector algorithm is presented which uses radar backscatter σ^0 measurements at two adjacent sub-scenes of RADARSAT-1 synthetic aperture radar (SAR) images, with each sub-scene having slightly different geometry. Resultant wind vectors are validated using in-situ buoy measurements, and compared with wind vectors determined from a hybrid wind retrieval model, using wind directions determined by spectral analysis of wind-induced image streaks, and observed by co-located QuikSCAT measurements. The hybrid wind retrieval model consists of CMOD-IFR2 (applicable to C-band, VV polarization) and a C-band co-polarization ratio according to Kirchhoff scattering. The new algorithm displays improved skill in wind vector estimation for RADARSAT-1 SAR data when compared to conventional wind retrieval methodology. In addition, unlike conventional methods, the present method is applicable to RADARSAT-1 images both with and without visible streaks. However, this method requires ancillary data such as buoy measurements to resolve the ambiguity in retrieved wind direction.**

***Index Terms*— Synthetic Aperture Radar (SAR), RADARSAT, Wind vector retrieval, Air-sea interaction**

I. Introduction

For incidence angles between 20° and 70°, the radar backscatter σ^0 from the ocean surface is caused by resonant Bragg scattering at the radar wavelength of a few centimetres. Despite modulation by both surface gravity waves and surface currents, these Bragg-scale waves are predominantly an oceanic response to the wind stress; therefore, ocean wind information may be extracted from synthetic aperture radar (SAR) images. The spatial resolution of the RADARSAT-1 SAR is 10 m to 100 m, while that of spaceborne scatterometers is in the 25 km to 50 km range. Therefore, the SAR can detect finer scale structures such as land-sea breezes, wakes, roll vortices, atmospheric gravity waves, and meteorological fronts. Moreover, the high resolution SAR-derived wind field may be particularly important in the coastal region, marginal ice zone, lakes and estuaries where scatterometer measurements are often contaminated by backscatter from land and ice (Vachon and Dobson, 2000; Portabella and Stoffelen, 2002).

Empirical C-band wind retrieval models such as CMOD-IFR2 relate the backscatter intensity at a particular frequency and polarization, the neutral wind speed at 10 m height, and the radar geometry, specifically the relative wind direction and incidence angle (Long, 1985; Stoffelen and Anderson, 1993; Quilfen, 1993; Vachon and Dobson, 1996). Originally proposed for backscatter measurements from the ERS C-band, VV polarization scatterometers, these models were later adopted to extract wind vectors from C-band SAR data. However, since radar backscatter σ^0 is a nonlinear function of both wind speed and direction, neither of these two parameters can be determined uniquely from a single backscatter measurement by SAR.

There are two main approaches to this under-determined problem: the SAR wind direction algorithm (SWDA) and the SAR wind algorithm (SWA). For SWDA, the wind direction is deduced from low wavenumber components of the SAR image spectra, which often appear in SAR ocean imagery as a result of boundary layer features such as wind rows or wind streaks (Brown 1990; Etling and Brown, 1993; Vachon and Dobson, 1996; Wackerman *et al.*, 1996; Fetterer *et al.*, 1998; Vachon and Dobson, 2000). The estimated wind direction is then used to infer the wind speed from the backscatter by using a CMOD-type model and incorporating an appropriate co-polarization ratio. A limitation of SWDA is that the SAR imagette size for spectral analysis should be at least ~16 km, roughly twice the expected maximum spatial scale of marine boundary layer roll vortices. Moreover, this method has an inherent 180° wind direction ambiguity. The SWA method, on the other hand, is based on the smearing of the SAR image by longer waves in the azimuthal direction (Chapron *et al.*, 1995; Kerbaol *et al.*, 1998). Application of SWA in nearshore and coastal areas is limited because shoaling and refraction of ocean waves can modify the radar backscatter induced by the local wind. Recently, Horstman and Koch (2005) estimated wind directions using the local spatial gradient of SAR image while Wackerman et al. (2003) used a projection method to generate wind direction estimates.

In this paper, we describe a new algorithm for wind retrieval from RADARSAT-1 images that is based on the methodology

Manuscript received June 16, 2006

Q. Zou is with Centre for Coastal Dynamics and Engineering, School of Engineering, University of Plymouth, Plymouth, Devon, PL4 8AA England (e-mail:qingping.zou@plymouth.ac.uk).

Y. He is with Institute of Oceanology, Chinese Academy of Sciences, Qingdao 266071, China

W. Perrie is with Fisheries & Oceans Canada, Bedford Inst. Oceanography, Dartmouth, Nova Scotia, B2Y 4A2 Canada and Dept. Engineering Mathematics, Dalhousie University, Halifax, Nova Scotia, B3J 1Y9 Canada

P. W. Vachon is with Defence R&D Canada – Ottawa, Ottawa, ON K1A 0Z4, Canada

used for scatterometer data. For the ERS-1 scatterometer, the wind speed and direction are inverted using a CMOD model and three σ^0 measurements collected by independent antennae pointing in different directions (Stoffelen and Anderson, 1997). Here, we extract the wind speed and direction simultaneously from two σ^0 measurements at adjacent wind cells within a single SAR image with slightly differing incidence angles. We assume that the wind speed and direction of the two cells are roughly equal to each other. Moreover, the resulting ambiguity in retrieved wind direction is eliminated by using the nearest buoy measurements.

Retrieved wind vectors from the new wind retrieval algorithm are validated with co-located NDBC buoy measurements, in comparison with the SWDA method, and in comparison with wind directions measured by co-located QuikSCAT data. In each case, a hybrid CMOD-IFR2 model function with a C-band co-polarization ratio according to Kirchhoff scattering is used.

II. Wind Retrieval Algorithm

Each RADARSAT-1 SAR image is first divided into 25 km × 25 km grid cells along the range and azimuth directions. The average backscatter and incidence angle are used to retrieve the wind speed and direction in each grid cell by using the hybrid model for C-band, HH polarization. The hybrid model consists of the CMOD-IFR2 model function (IFREMER-CERSAT, 1996):

$$\sigma_{VV}^0 = A + B\cos\phi + C\cos 2\phi , \qquad (1.1)$$

where the subscript VV denotes the polarization, ϕ is the wind direction relative to the radar-look direction (ϕ=0° when wind blows toward the radar), A, B and C are empirical coefficients that depend on the radar incidence angle θ, and the 10 m wind speed U, and the Kirchhoff co-polarization ratio (Elfouhaily *et al.*, 1999)

$$P_r = \left(\frac{1+\tan^2\theta}{1+2\tan^2\theta} \right)^2 . \qquad (1.2)$$

Combining equations (1.1) and (1.2) yields

$$\sigma_{HH}^0 = P_r \sigma_{VV}^0 , \qquad (1.3)$$

where the subscript HH represents the polarization (hereafter omitted for simplicity).

We label each grid cell (m, n) where m and n index the range and azimuth coordinates, respectively. The wind vector for cell (m, n) is retrieved by minimizing the cost function $J_{m,n}$, which is a sum of the error between the observed and estimated backscatter in two adjacent wind cells, i.e., (m, n) and ($m+1$, n), each with slightly differing incidence angles:

$$J_{m,n} = \left(\sigma_{m,n}^0 - \hat{\sigma}_{m,n}^0\right)^2 + \left(\sigma_{m+1,n}^0 - \hat{\sigma}_{m+1,n}^0\right)^2 , \qquad (1.4)$$

where $\sigma_{m,n}^0$ and $\sigma_{m+1,n}^0$ are the observed backscatter, $\hat{\sigma}_{m,n}^0 = \hat{\sigma}_{m,n}^0(U_{m,n}, \phi_{m,n})$ and $\hat{\sigma}_{m+1,n}^0 = \hat{\sigma}_{m+1,n}^0(U_{m+1,n}, \phi_{m+1,n})$ are the estimated backscatter from the hybrid model described by equations (1.1) to (1.3), which are functions of wind speeds $U_{m,n}$, $U_{m+1,n}$ and wind directions $\phi_{m,n}$, $\phi_{m+1,n}$. Neglecting differences between the wind vectors of adjacent cells, namely $\phi_{m+1,n} = \phi_{m,n}$ and $U_{m+1,n} = U_{m,n}$, and minimizing equation (1.4), we obtain

$$\frac{\partial J_{m,n}}{\partial \phi_{m,n}} = 0 \qquad (1.5)$$

and

$$\frac{\partial J_{m,n}}{\partial U_{m,n}} = 0 . \qquad (1.6)$$

For simplicity, we drop the subscript (m, n) hereafter. For a given wind speed and incidence angle, the radar backscatter σ^0 is a second order polynomial function of $\cos\phi$, as shown by the CMOD model of equation (1.1). Therefore, the cost function J and its derivatives $(\sin\phi)^{-1}\partial J/\partial\phi$ and $\partial J/\partial U$ are third and fourth order polynomial functions of $\cos\phi$. Each of equations (1.5) and (1.6), therefore, leads to four solutions of $\cos\phi$ for a given wind speed U.

In practice, we solve equations (1.5) and (1.6) numerically with the following procedure:

a) Start with a trial wind speed U =2 m/s for a particular grid cell, substitute it into equations (1.5) and (1.6) to obtain $\cos\phi$;
b) calculate the discrepancy between the solutions of $\cos\phi$ from equations (1.5) and (1.6);
c) select those values with a discrepancy that is smaller than a user-specified tolerance (the final results of retrieved wind are not sensitive to the tolerance value);
d) increase the trial wind speed U in increments of 0.5 m/s and repeat the procedure until U reaches 30 m/s, the expected upper limit for CMOD model functions;
e) among all trial wind speed values, select the 12 pairs of $\cos(\phi)$ and U that give the smallest discrepancy, constituting optimum wind vectors for that particular grid cell.

Finally, among the multiple solutions for the wind direction, we choose the wind direction that aligns best with the nearest buoy wind direction. For wind cells at the edge of an image, wind vectors are taken to be the same as those of the nearest wind cell along the range direction. A similar methodology was applied to VV-polarization ENVISAT ASAR images by He *et al.* (2005), including a detailed discussion of the constraints of the methodology. The present paper extends those results to RADARSAT-1 data through use of a co-polarization ratio, and presents new validation results.

III. Numerical Simulation

For scatterometers such as on QuikSCAT or ERS-1/2, wind vectors are retrieved from the radar backscatter observed at multiple azimuth looks. Here, for RADARSAT-1, wind vector are retrieved from the radar backscatter observed in neighboring sub-images at slightly different incidence angles. Since the cost function depends on both wind vectors and incidence angles, we are concerned with the change in wind direction sensitivity with incidence angle. The following two numerical simulations are sensitivity studies to show the

advantages and disadvantages of applying the present method to RADARSAT-1 data.

Assuming a wind speed of 8 m/s and a wind direction of 45° (which is the wind direction relative to the radar look direction: this angle is zero when the wind is blowing towards the radar), the corresponding radar backscatter pairs are σ_2^0 and σ_1^0 at neighboring sub-images with incidence angles of 35° and 36°. Assuming these radar backscatter pairs, σ_1^0 and σ_2^0, are SAR-observed values, the relationship between the cost function and the wind speed and direction are shown by the contour plot in Fig. 1. There are 8 local cost function minima, as indicated by the black specks in the plot. These lead to the wind vector solutions listed in Table I. Similar to scatterometer methodology, multiple solutions may exist in the present wind retrieval for RADARSAT data. However, wind retrieval from scatterometers is subject to little ambiguity because the QuikScat best fit solution is correct in 80% of the cases and 3rd and 4th solutions occur in a minority of cases, while the ERS scatterometers provide two solutions that are almost exactly 180° apart (Portabella 2002). The direction ambiguity associated with scatterometers is much easier to resolve than that posed here. Moreover, multiple azimuth angles are more effective in obtaining wind direction than multiple incidence angles. Therefore, we are forced to eliminate the multiple solutions by using ancillary wind direction data, such as buoy data.

In our example, given a 45° reference wind direction, Table I implies that the resultant wind speed is 6.9 m/s, and the wind direction is 32°, because this combination gives a wind direction that is closest to the actual wind direction.

Through numerical experiments on model sensitivity to noise similar to those in He et al. (2005), we found that errors in wind speed lead to very small errors in wind direction. However large errors in retrieved wind direction may occur if wrongly referenced wind directions are used to choose from among the multiple wind direction solutions.

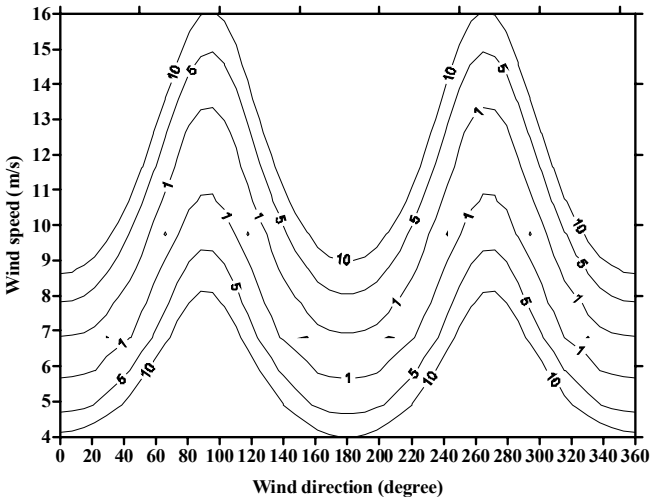

Fig. 1. Cost function contours as a function of wind speed and wind direction. Eight local minima are indicated by the black specks.

TABLE I

WIND VECTORS OBTAINED FROM THE NUMERICAL SIMULATION

Number	1	2	3	4	5	6	7	8
Wind speed (m/s)	6.7	6.7	6.9	6.9	9.6	9.6	9.6	9.6
Wind direction (°)	155	205	32	328	63	297	121	239
Cost function ($X\ 10^{-2}$)	1.46	1.46	1.26	1.26	1.37	1.37	1.60	1.60

IV. MODEL VERIFICATION

A set of five C-band, HH polarization RADARSAT-1 images was used to validate our new wind retrieval algorithm. They were acquired over the Bay of Fundy, the northeast and northwest coasts of the US, and the east coast of Canada between 25 December 2002 and 13 March 2003. Wind vectors were estimated using the new wind algorithm, with the ambiguity in retrieved wind direction eliminated using the nearest operational buoy measurements. The results were compared with those calculated by combining the wind directions predicted by SWDA (Vachon & Dobson 2000) and observed by co-located QuikSCAT measurements, using the hybrid model of equations (1.1) to (1.3). However, we excluded low wind conditions (< 4 m/s), for which the CMOD-IFR2 relationship is not valid because patchiness, fronts and slicks can have significant effects on the radar backscatter amplitude (Fetterer *et al.*, 1998).

The wind speed estimates from our new algorithm are compared with those obtained using the wind direction given by the spectral analysis of the SAR images (i.e., SWDA) in combination with the hybrid model from equations (1.1) to (1.3), in relation to *in situ* buoy measurements (Fig. 2a). The 180° wind direction ambiguity associated with SWDA was removed by using the nearest buoy wind direction. Associated wind direction comparisons are presented in Fig. 2c. A discrepancy in wind direction leads to a misinterpretation of wind speed using the hybrid model, which increases at higher wind speeds. Therefore, the RMS error in wind direction is more suitable for evaluating the wind retrieval algorithm. The RMS wind direction error from our new wind algorithm is about half that reported by Fetterer *et al.* (1998), whereas RMS wind direction errors from the SWDA method and Fetterer *et al.* (1998) are comparable (Table II).

Fig. 2b compares wind speeds retrieved by our new algorithm with those obtained using the wind directions from co-located QuikSCAT measurements (with a acquisition time difference of between 30 and 60 minutes), using the hybrid model of equations (1.1) to (1.3). The comparisons were conducted in relation to *in situ* buoy measurements. Associated wind direction comparisons are given in Fig. 2d. Errors in wind retrieval using the wind directions from co-located QuikSCAT data are comparable to those obtained by the SWDA method in this study and by Fetterer *et al.* (1998), but they are considerably higher than those resulting from our new algorithm (Table II).

The estimated wind vectors from our new algorithm are compared with those from the SWDA method for the SAR

image of 21 January 2003 in Fig. 3. As indicated by Fig. 3, the wind directions given by SWDA are biased to the right, compared to those predicted by our new algorithm. Deviations in wind speed estimates in Fig. 3 are solely due to the differences in the wind direction estimates. Wackerman *et al.* (1996) and Alpers and Brümmer (1994) found that the wind streak directions determined by SWDA are not perfectly aligned with the actual wind direction.

Fig. 4 compares the estimated wind vectors from our new algorithm with those extracted from wind directions of co-located QuikSCAT measurements (with a time lag of 37 minutes) using the hybrid model of equations (1.1) to (1.3). Fig. 5 show a comparison of wind speed and direction for the three sets of wind vectors in Figs. 3 and 4. As shown by these figures, the wind speed and direction estimated by SWDA are biased low relative to those of our new wind algorithm, whereas those inferred from co-located QuikSCAT directions compare well with those obtained by the new wind algorithm. In Fig. 5, we excluded wind vectors from grid cells on land, or having incidence angles smaller than 23° (the CMOD type models were developed for incidence angles larger than 23°).

V. Conclusion and discussions

We have constructed a wind retrieval algorithm for C-band, HH-polarized RADARSAT-1 SAR images. The algorithm can be adapted for wind vector estimates for other C-band SAR images. The new algorithm results in a RMS error of 3.6 m s^{-1} in wind speed and 17° in wind direction, for moderately wind speeds between 13 and 22 m s^{-1}. By comparison, the conventional SWDA method (Vachon & Dobson 2000) has a RMS error of 3.6 m s^{-1} in wind speed and 38° in wind direction, whereas wind retrieval using the wind directions from co-located QuikSCAT data resulted in a RMS error of 3.9 m s^{-1} in wind speed and 35° in wind direction. For lower wind speeds, between 4 and 16 m s^{-1}, Fetterer *et al.* (1998) obtained a RMS error of 2 m s^{-1} in wind speed and 37° in wind direction.

In previous approaches to wind retrieval, such as SWDA and SWA, either wind speed or wind direction can be retrieved from SAR measurements, but not both. By comparison, wind speed and direction are extracted simultaneously in our new wind algorithm. In addition, the present algorithm does not rely on the presence of visible wind streaks. Therefore, our new algorithm can potentially be automated for wind retrieval from RADARSAT SAR images. Moreover, our new wind algorithm has the potential to retrieve wind at higher resolutions than conventional algorithms. This is of particular importance for investigations of boundary layer rolls in hurricanes, for example.

The five images used in this study have relatively homogeneous and uniform wind conditions. Therefore, the 180° wind directional ambiguity was successfully resolved. However, in cases involving more complicated mesoscale features, such as hurricanes or intense small cyclones in which rapid spatial and temporal variations of wind direction prevail, resolving the 180° ambiguity may be quite challenging. Existing methods that remove the wind direction ambiguity in scatterometer images, such as those proposed by Stofellen and Anderson (1997), may offer a conceptual methodology.

The errors in wind direction and the radiometric noise in the SAR data lead to larger errors in wind speed at a higher wind speed. Thus, they constitute the major sources of error in wind retrieval because the wind speeds used in this study exceed 13 m s^{-1}. In the special cases of up-, cross- and down-wind orientations, when $\cos(\phi)$ and $\cos(2\phi)$ are -1, 0 or 1, the sensitivity of the present wind retrieval algorithm to wind direction is close to zero (see Fig. 1). Changes in wind speed and direction in the neighboring sub-images also introduces errors. Other than the discrepancy inherent with the wind retrieval algorithm, additional sources of error include: (1) limitations on buoy measurement accuracy by about ±0.8 m s^{-1} and ±10° (Gilhousen 1987); (2) limited calibration accuracy of RADARSAT-1, especially in the coastal zone; (3) space and time separations between the center of wind cells and buoy observations; (4) local non-wind effects on the backscatter by ocean fronts and slicks; and (5) close proximity of buoys to the coast.

Acknowledgment

We thank John Wolfe (Canada Centre for Remote Sensing) for providing us with the CCRS wind retrieval (spectral analysis-based) software package for RADARSAT-1 SAR images. We were funded by Petroleum Research Atlantic Canada, the Canadian Space Agency, and Canada Panel on Energy Research and Development.

References

[1] Alpers, W. and B. Brümmer, Atmospheric boundary layer rolls observed by the synthetic aperture radar aboard the ERS-1 satellite, J. Geophys. Res., 99, 12613-12621, 1994.

[2] Brown, R. A., Surface fluxes and remote sensing of air-sea interactions, in surface waves and fluxes, edited by G. L. Geernaert and W. J. Plant, pp. 7-27, Kluwer Acad., Norwell, Mass., 1990.

[3] Chapron, B., T.T. Elfouhaily, and V. Kerbaol, Calibration and validation of ERS wave mode products, DRO/OS/95-02, Inst. Fr. De Rech. Pour l'Exploit. De la mer, Brest, France, 1995.

[4] Elfouhaily, T., D. R. Thompson, D. Vandemark, and B. Chapron, A New bistatic model for electromagnetic scattering from perfectly conducting random surfaces, Waves in Random Media, 9, 281-294. 1999.

[5] Etling, D., and R. A. Brown, Roll vortices in the Planetary boundary layer: A review, Boundary Layer Meteorology, 65, 215-248, 1993.

[6] Fetterer, F., D. Gineris, and C. C. Wackerman, Validating a scatterometer wind algorithm for ERS-1 SAR, IEEE Trans. Geosci. Remote Sens., Vol. 36, 479–492, 1998.

[7] He, Y.-J., W. Perrie, Q.-P. Zou and P.W. Vachon, A new wind vector algorithm for C-band SAR, IEEE Trans. Geosci. Remote Sens., 43 (7), 1453-1458, 2005.

[8] Horstmann, J. and Koch, W., Measurement of ocean surface winds using synthetic aperture radars, IEEE Journal of Oceanic Engineering, Vol. 30, No. 3,508-515, 2005.

[9] IFREMER-CERSAT Off-line wind scatterometer ERS products: user manual, Technical Report C2-MUT-W-01-1F, Version 2.0, IFREMER-CERSAT, BP 70, 29280 PLOUZANE, France.

[10] Long, A.E. Towards a C-band radar sea echo model for the ERS-1 scatterometer in Proc. 3rd International Colloquium on Spectral Signatures of Objects in Remote Sensing, Les Arcs, France, 16-20 Dec., ESA SP-247, pp 29-34, 1985.

[11] Kerbaol, K., B. Chapron, and P.W. Vachon, Analysis of ERS-1/2 synthetic aperture radar wave mode imagettes, J. Geophys. Res., vol. 103, no. C4, 7833–7846, 1998.

[12] Portabella, M., and A. Stoffelen, Toward an optimal inversion method for synthetic aperture radar wind retrieval, J. Geophys. Res., vol. 107, no. C8, 10.1029/2001JC000925, 2002.
[13] Portabella, M. Wind Field retrieval from Satellite Radar Systems, Ph.D thesis, ISBN:90-6464-499-3, University of Barcelona, 2002.
[14] Quilfen, Y. ERS-1 off-line wind scatterometer products. Technical Report ERS-SCAT/IOA/DOS-01, IFREMER. 1998.
[15] Stoffelen, A., and D. Anderson, ERS-1 scatterometer data characteristics and wind retrieval skill, Adv. Space Res., 13, 553-560, 1993.
[16] Stoffelen, A., and D. Anderson, Scattermeter data interpretation: Measurement space and inversion, J. Atmos. Oceanic. Technol., 14(6), 1298-1313, 1997.
[17] Vachon, P. W. and F. W. Dobson, Validation of wind vector retrieval from ERS-1 SAR images over the ocean, Global Atmos. Ocean Syst., vol. 5, 177–187, 1996.
[18] Vachon, P.W. and F.W. Dobson, Wind retrieval from RADARSAT SAR images: Selection of a suitable C-band HH polarization wind retrieval model, Can. J. Remote Sensing, vol. 26, 306–313, Aug. 2000.
[19] Wackerman, C., C. Rufenach, R. Shuchman, J. Johannessen, and K. Davidson, Wind vector retrieval using ERS-1 synthetic aperture radar imagery, IEEE Trans. Geosci. Remote Sensing, vol. 34, 1343–1352, Nov. 1996.
[20] Wackerman, C., W. G. Pichel, and P. Clement-Colón, A projection method for automatic estimation of wind vectors with RADARSAT SAR imagery, Proceedings of the second workshop on coastal and marine applications of SAR, Svalbard, Norway, 8-12 September, 2003.

TABLE II
COMPARISONS OF BUOY WINDS WITH ESTIMATES FROM NEW ALGORITHM, WIND DIRECTIONS BY THE SPECTRAL ANALYSIS AND CO-LOCATED QUIKSCAT DATA.

Parameters	Wind speed (m/s)		Wind direction (°)	
Error	Mean	RMS	Mean	RMS
New algorithm	-1.49	3.5	0.43	16.6
FFT	0.44	3.6	-7.6	38.0
QuikSCAT	1.95	3.9	1.4	34.6

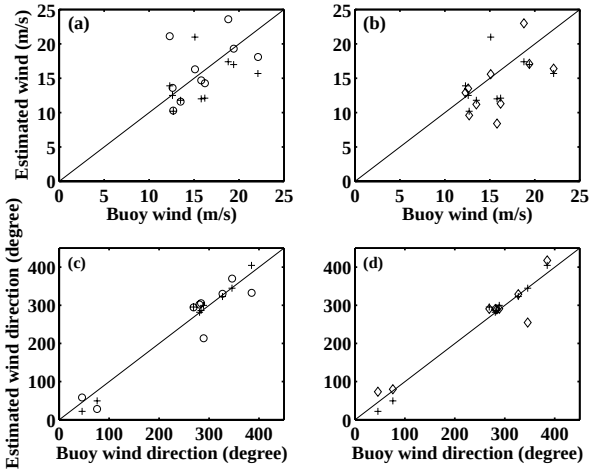

Fig. 2. Comparisons of three sets of estimated wind vectors with *in situ* buoy data: (a) & (b) wind speeds; and (c) & (d) wind directions. These sets are: our new wind retrieval algorithm (+); wind retrievals using the wind directions from spectral analysis of SAR images (o); and co-located QuikSCAT measurements (◊).

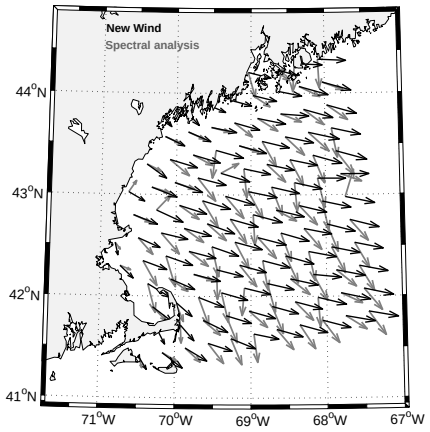

Fig. 3. Estimated wind field for the RADARSAT-1 SAR image of 21 January 2003 by the new wind retrieval algorithm (black); using the estimated wind directions from spectral analysis of SAR images (gray).

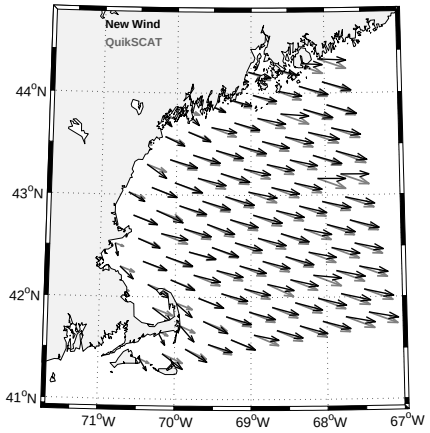

Fig. 4. As in Fig. 3, using the wind directions of co-located QuikSCAT measurements (gray).

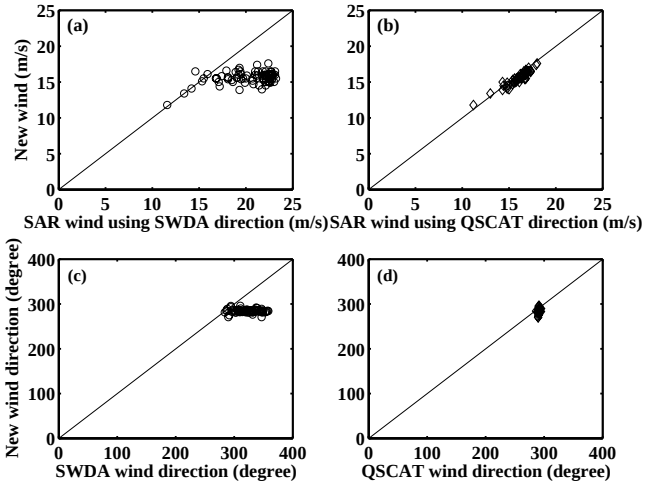

Fig. 5. Estimated (a) & (b) wind speeds and (c) & (d) wind directions for the SAR image of 21 January 2003 by the new wind retrieval algorithm (black arrows in Fig. 3) versus those using the wind directions: (left panel) estimated from spectral analysis of SAR images (gray arrows in Fig. 3); (right panel) observed by co-located QuikSCAT measurements (gray arrows in Fig. 4).